Temperature controlled properties of sub-micron thin SnS films

*Stephen N. Nwankwo[1], Stephen Campbell[1], Ramakrishna K.T. Reddy[2], Neil S. Beattie[1], Vincent Barrioz[1] and Guillaume Zoppi[1,]**

1. Department of Mathematics, Physics and Electrical Engineering, Northumbria University, Ellison Building, Newcastle upon Tyne, NE1 8ST, UK

2. Department of Physics, Sri Venkateswara University, Tirupati-517502, India.

**Guillaume.zoppi@northumbria.ac.uk, tel: +44(0) 191 2437013*

Abstract

Tin sulphide (SnS) thin films deposited by thermal evaporation on glass substrates are studied for different substrate temperatures. The increase in substrate temperature results in the increase of the crystallite size and change in orientation of the films. The crystal structure of the film is that of SnS only and for temperatures ≤ 300 ºC the films are of random orientation, whereas for higher temperatures the films become (040) oriented. The variation of Sn/S composition was accompanied by a reduction in optical energy bandgap from 1.47 to 1.31 eV as the substrate temperature increases. The Urbach energy was found stable at 0.169 ± 0.002 eV for temperature up to 350 °C. Photoluminescence emission was observed only for films exhibiting stoichiometric properties and shows that a precise control of the film composition is critical to fabricate devices while an increase in grain size will be essential to achieve high efficiency.

Keywords: Thermal evaporation, thin films, tin sulphide, photoluminescence, solar cells.

1. Introduction

Research in thin films solar cells is focusing towards developing alternative absorbing materials that are low-cost, non-toxic, earth abundant and easy to fabricate. Tin Sulphide (SnS) is such a candidate for making cost effective solar cells having demonstrated good optical properties [1], ideal direct bandgap for photon absorption (in the range of 1.3-1.5 eV) [2], an appropriate hole mobility (0.8-15.3 $cm^2V^{-1}s^{-1}$) and a good carrier concentration (10^{16} cm^{-3}) [1], and with both Sn and S available in large abundance [3]. Those ideal properties are further supported with theoretical calculations indicating realistic conversion efficiency in the range of 24-31% for SnS solar cells [4, 5]. However the maximum efficiency reported for SnS solar cells to date is only 4.4% [6]. There are several factors that currently contribute this relative poor performance compared to other chalcogenide thin film photovoltaics. Firstly the concentration of defects in the SnS thin film layers arising from deposition condition and

methods can create excessive Shockley-Read-Hall recombination centres [3, 7]. This is also linked to non-stoichiometric composition and structural inhomogeneity arising from different crystal orientation of SnS grains or crystallites that can lead to different optical behaviour of the SnS layers [8], which may limit the performance of the SnS-based solar cells. Secondly, the pn junction formation and in particular the perfect matting n-type material has not yet been revealed. The record efficiency device was produced using a Zn(O,S) buffer and judged adequate with reduced band offset at the interface with SnS [6]. Sugiyama *et al.* study a broad range of possible n-type material for SnS using photoelectron yield spectroscopy and concluded that type I heterostructures could only be achieved with ZnIn2Se4 and MgxZn1-xO buffer layer with the latter one being the most appropriate [9]. Finally, the ability to create a good p-n junction will also depend on crystallographic orientation of the SnS absorber layer [10] which is controlled by the deposition parameters.

Several techniques have been reported in the deposition of thin films of SnS which include spray pyrolysis [11], electro deposition [12], chemical bath deposition (CBD) [13], plasma-enhanced chemical vapour deposition [14], thermal evaporation either short or long-throw [15-18], hot wall deposition method [19], pulsed chemical vapour deposition [20] and atomic layer deposition [ALD] [1,20]. Physical vapour deposition (PVD) techniques such as thermal evaporation are reliable, easy to control and provide a great level of process parameter variations. PVD is the method of choice for depositing thin film inorganic absorber reaching power conversion >20% (see for example $CuInGaSe_2$ (CIGS) and CdTe record efficiencies ≥22% [21]). Structural parameters (such as crystallite size, strain and degree of orientation) and optoelectronic parameters (such as absorption coefficient, energy bandgap, refractive index and extinction coefficient) of SnS thin films prepared with some of these techniques have been reported [1,15,16]. Devika *et al.* investigated the dependence of SnS properties on film thickness and demonstrated that improved crystallinity of the layers can be achieved for film thickness >0.75 µm [15]. While the record SnS device used an absorber thickness of only 500 nm such a thin absorber is likely to limit the overall performance. Indeed for CIGS solar cells short circuit current, fill factor and as results efficiency, seriously deteriorate for film thicknesses below 800nm [22-24]. Here, we present detailed structural and optical properties of sweat spot (<1 µm) thermally evaporated thin films and demonstrate that luminescence material can only be produced with a precise control of the film stoichiometry and crystallographic orientation.

2. Experimental

SnS absorber layers were grown via thermal evaporation of 5N purity SnS pellets (Testbourne T7-5014-M) onto pre-cleaned soda lime glass (SLG) substrate. The SLG substrates were cleaned chemically (dilute decon-90 solution with deionised water) followed by ultrasonication (water for 15 minutes) prior to the deposition. All the layers were deposited at high vacuum (< $1x10^{-6}$ mbar) at substrate temperature in the range 200-400 ^{o}C with thickness of 0.9 ± 0.1 µm (deposition rate of 3 nms^{-1}). The source substrate distance and substrate rotation were set at 300 mm and 10 rpm respectively.

The composition, structure and optical properties of the as-deposited layers were studied. Siemens D5000 X-ray diffractometer in Bragg-Brentano configuration using a CuK_{α} (λ = 1.54 Å) radiation source was used to study the layers orientation and crystallographic structures. Scanning electron microscopy (SEM) (Tescan Mira3) and energy dispersive X-ray spectroscopy (EDS) (Oxford Instruments) were used to investigate the morphology and composition of the as-deposited layers, respectively. Optical transmittance and reflectance of the layers were examined in the 300-1400 nm wavelength range with a Shimadzu UV-VIS-2600 spectrophotometer. The Raman spectra were studied with a Horiba Labram 300 Raman spectrometer of 632.8 nm wavelength using a HeNe laser. Secondary ion mass spectroscopy (SIMS) was performed using a primary beam of oxygen ions (5 kV, 300 nA) rastered over a 0.5 x 0.5 mm^2 area (gating 10%) and quadrupole detector from Hiden Analytical. The PL spectra were measured using a Horiba Jobin Yvon iHR320 spectrometer with a cooled InGaAs detector coupled to a lock-in amplifier. A 532 nm continuous wave diode-pumped solid-state laser was used as an excitation source.

3. Results and Discussion

The composition of the as-deposited SnS films (see table 1) showed gradual increase of the Sn/S ratio in the films with substrate temperature, whereas the starting material (pure SnS pellets) had a stoichiometric composition of tin and sulphur (Sn/S = 1.00). The Sn/S range of 0.96 - 1.10 shows a trend of decreasing S content in the thin films as the substrate temperature increases in agreement with previous work [16, 25]. The change in composition with growth conditions are due to re-evaporation at the surface of the growing films where the vapour pressure of S increases with temperature faster than that of Sn, (e.g. the vapour pressure of sulphur P_S and tin P_{Sn} is $1.0x10^{-2}$ mbar at 102 ^{o}C and 1224 ^{o}C, respectively,

giving a very large 1122 ºC temperature difference) [26]. The composition uniformity with respect to the film thickness was probed by SIMS and is shown in figure 1 where the intensity ratio of Sn and S ions are plotted for three films. All films showed uniform profiles with depth of both Sn and S but the ratios showed the films becoming increasing Sn rich as substrate temperature increases in good agreement with the EDS data shown in table 1.

Table 1: SnS thin film composition across the substrate temperature range along with key optical properties. The starting SnS evaporant material was measured at Sn/S = 1.00 using EDS. The energy bandgap E_g and Urbach energy E_u were determined from optical measurements.

Substrate temperature (ºC)	**Sn (at %)**	**S (at %)**	**Sn/S**	E_g **(eV)**	E_u **(eV)**
200	48.9	51.1	0.96	1.46	0.167
250	49.2	50.8	0.97	1.43	0.169
300	49.7	50.3	0.99	1.41	0.171
325	49.8	50.2	0.99	1.40	0.172
350	50.9	49.1	1.00	1.37	0.170
400	52.4	47.6	1.10	1.31	0.186

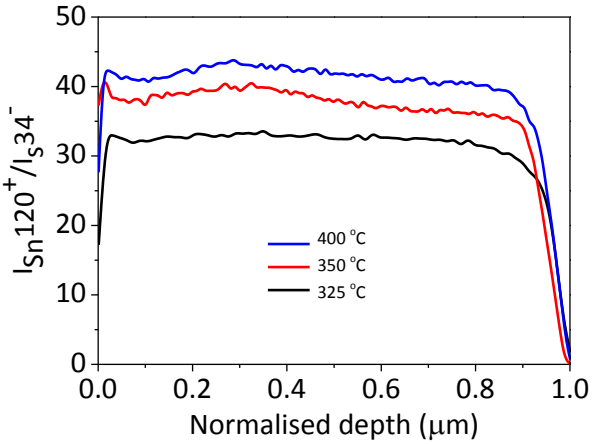

Figure 1: Variation of Sn/S ratio with film depth as determined from SIMS for substrate temperature of 325, 350 and 400 ºC.

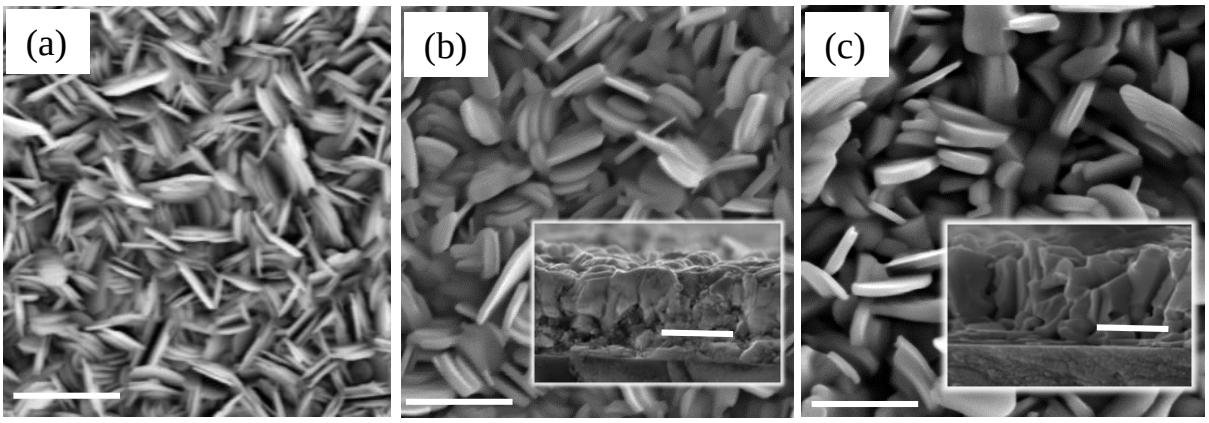

Figure 2: SEM micrographs (5kV) of as-deposited SnS films at substrate temperature of (a) 200, (b) 300 and (b) 350 ^{o}C, inset: cross-section (scale bars denote 500 nm).

The surface morphology of as-deposited films shows randomly oriented rice and flake-like grains that are dependent on substrate temperature: as substrate temperature increases, the micrographs reveal the growth of bigger grains as shown in figure 2 (a-c). Further increase in temperature yielded no visual change on the surface morphology. The cross-sectional views of the as-deposited SnS layers (inset of figure 2 (b and c)), confirmed the small grained structure with some columnar feature appearing at temperature ≥ 350 °C. Quantification of grain size was not possible due to non-uniform arrangement of grain distribution, however the grain size increase is visually noticeable from both planar and cross sectional views. The bigger grains are likely due to the increase in adatoms mobility with temperature, promoting coalescences of the smaller grains to form bigger grains. However, the growth of large grains in the 3-dimensional space is required to reduce carrier recombination usually associated with polycrystalline thin film absorber.

The transmittance, *T*, and reflectance, *R*, spectra of the as-deposited SnS thin films studied over the wavelength range of 300-1400 nm are plotted in figure 3a. A sharp fall of the transmittance was observed for all films at the wavelength regarded as the fundamental absorption edge. The absorption edge shifts towards longer wavelength with increase in substrate temperature, and this is associated with the change in composition described earlier. The spectra also show good absorption in the visible range where the transmittance is close to zero. The absorption coefficient (α) is calculated using the relation [27]:

$$\alpha = -\left(\frac{1}{x}\right) \ln \left(\frac{[(1-R)^4 + 4T^2R^2]^{\frac{1}{2}} - (1-R)^2}{2TR^2} \right) \quad (1)$$

where x is the film thickness. The films show high absorption coefficient of 3.5 x 10^4 to 1.2 x 10^{-5} cm^{-1} (at wavelength range 300-670 nm). The optical energy bandgap (E_g) was calculated using the relation:

$$\alpha h\nu = c\left(h\nu - E_g\right)^a \qquad (2)$$

where c is a constant called the band tailing parameter, ($h\nu$) is the photon energy, a is used as ½ or 2 for direct and indirect allowed transitions, respectively. Both direct and indirect bandgap values have been reported for SnS thin films depending on preparation and growth conditions [16, 28-30]. In this study, the plot of $(\alpha h\nu)^2$ vs $(h\nu)$ (see figure 3b) gave a best straight line fit for a = ½ and the bandgap was determined by extrapolating the linear region to the $h\nu$ axis. The plots for a = 2 are shown in the figure S1a for reference. The direct bandgap energy range of 1.31-1.47 eV (see Table 1) are recorded for the different substrate temperatures with varying Sn/S atomic composition. The near stoichiometric SnS film (Sn/S = 1.00) grown at 350 ºC substrate temperature has a direct bandgap of 1.37 eV. This value is close to the reported bandgap of stoichiometric polycrystalline SnS, 1.35 eV [16]. The noticeable change in the bandgap with the substrate temperature is linked to the changing composition of the films.

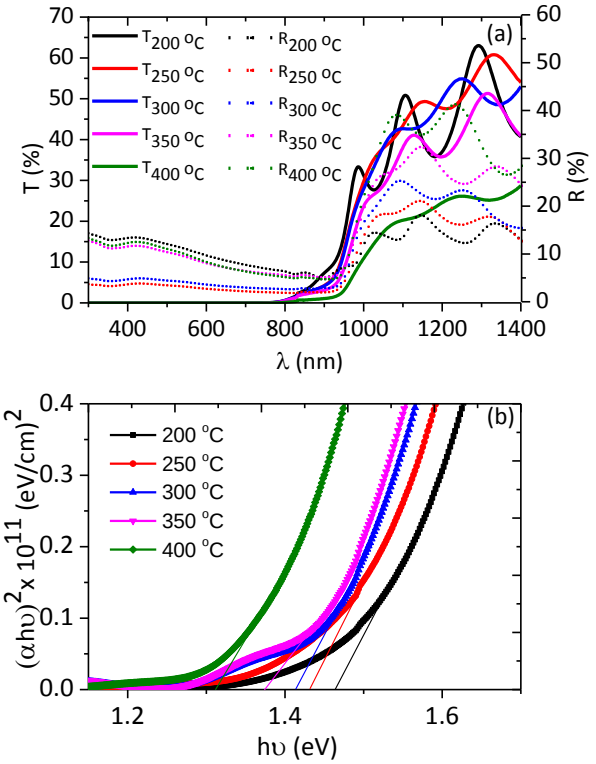

Figure 3: (a) Transmittance (solid lines) and reflectance (dotted lines) versus wavelength and (b) $(\alpha h\nu)^2$ versus $h\nu$ of the as-deposited SnS thin films on SLG.

In thin films materials, the exponential dependence of absorption coefficient (α) on the photon energy can give information on the localized states that tail off from the band edge with the optical bandgap. Below the optical band edge, the relationship between (α) and photon energy ($h\nu$) is following the Urbach empirical rule (see figure S1b) [31, 32]. This rule characterises the degree of the absorption edge spreading due to the crystalline lattice disorder resulting from structural anomalies and compositional disordering. For single crystal, the fluctuations of atomic position during thermal vibration at high temperatures determines the nature of the tail state. The Urbach rule is given as [31]:

$$\alpha = \alpha_o \exp\left(\frac{h\nu}{E_u}\right) \quad (3)$$

where α_o denotes a pre-exponential term which is constant and E_u is Urbach energy which indicates the width of the exponential absorption edge. From the plot of *ln* (α) against ($h\nu$) (shown in figure S2) near the absorption edge for the as-deposited SnS films at different substrate temperature, the Urbach energy were estimated as the inverse of the slope. The E_u value is ranging from 0.167 to 0.186 eV across the temperature range as listed in table 1. For temperature of 250-350 ^oC, E_u is invariant (within the experimental error) while a large increase is observed for the highest temperature. This correlates well with the increase in Sn/S ratio (10% at 400 ^oC) resulting in an increase in the disordered atoms and defects in the structural bonding that can cause the absorption edge to spread at the lower region [32] and is the main reason for the observed variations.

Figure 4a shows the X-ray diffraction (XRD) spectra of the as-deposited SnS thin films grown at substrate temperature ranging from 200 to 400 ^oC. XRD analysis showed the films were highly crystallized with properties matching well with orthorhombic structure of SnS (Herzenbergite) consistent with the reference powder diffraction file 039-0354. The layers were all single phase (also confirmed from the Raman analysis as detailed later) with the (111)/(040) planes giving rise to the most prominent peak. The (111) reflections are more likely associated with lower substrate temperatures while the (040) reflections are related to higher substrate temperatures. This is consistent with other reports [15, 16, 28, 33 and 34]. Raman studies were also conducted to further complement the XRD data (see figure 4b). Three main peaks are evident in the Raman spectra, which are located at 140, 167 and 196

cm^{-1} and a minor peak found at 98 cm^{-1}, these can be attributed to SnS [35, 36]. No peak belonging to Sn_2S_3 (307 cm^{-1}) and SnS_2 (312 cm^{-1}) [37] are detected within the analysis effective depth (depth = 147 nm) therefore it can be concluded that the crystal structure of the film is that of SnS only. The most intense peak for the samples is at 167 cm^{-1} for all the substrate temperatures and corresponds to B_{2g} mode of SnS while peaks at 98 and 196 cm^{-1} are from the A_g modes [35].

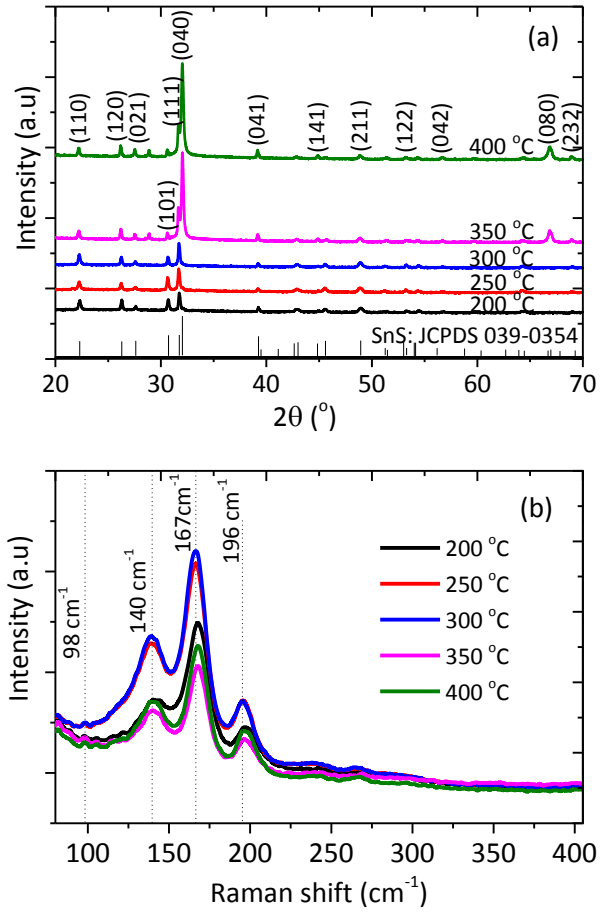

Figure 4: (a) XRD and (b) Raman spectra of SnS films grown across the substrate range.

The preferred orientation of the crystals σ in the as-deposited polycrystalline SnS films were established by first calculating the texture coefficient (C_{hkl}) [38]. The C_{hkl} and σ values are included in the supplementary information table S1. Figure 5a shows the variation of $C_{(111)}$, $C_{(040)}$ and σ as a function of substrate temperature. For temperatures ≤300 °C the films are random, whereas for the higher temperatures the films become (040) oriented.

Crystallite size and strain were also estimated from the XRD data. The strain may arise due to lattice mismatch or difference between thermal coefficient of the glass substrate and growing film, which can lead to a shift in the peak position as well as peak broadening. To estimate

the average crystallite size (D), Williams-Hall (W-H) method [39] was employed using the following equation:

$$\beta\cos\theta = \frac{0.94\lambda}{D} + 4\varepsilon\sin\theta \qquad (4)$$

where ε is strain, λ is the wavelength of the X-ray radiation (1.54 Å), β is the full width half maximum (FWHM) of the diffraction peaks and θ is the Bragg angle. All eight peaks shown in table S1 were used for the calculations. From the plot of $\beta\cos\theta$ against $4\sin\theta$, the strain was extrapolated from the slope of the graph, while the intercept was used to calculate the average crystallite size. The plot of average crystallite size and strain against the substrate temperature is shown in figure 5b.

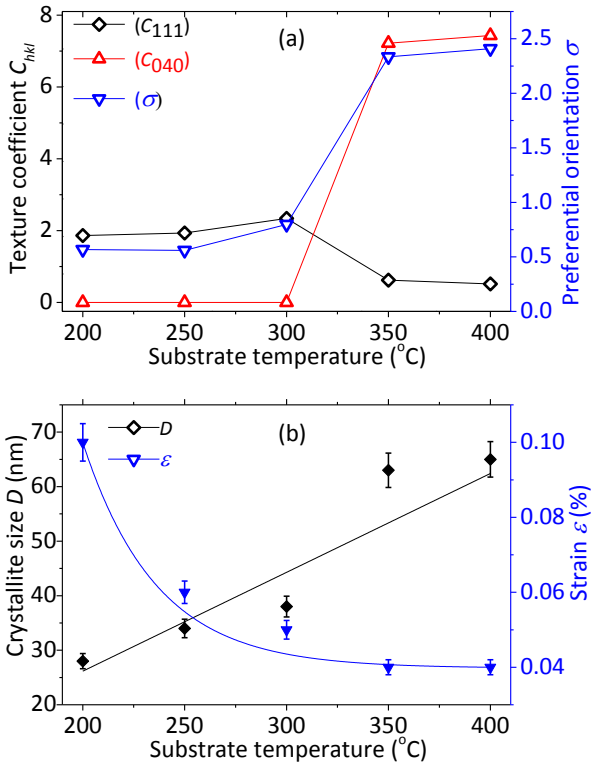

Figure 5: (a) variation of texture coefficient $C_{(111)}$ and $C_{(040)}$ and degree of preferred orientation σ with temperature, (b) variations of crystallite size and strain with substrate temperature (the lines are guides for the eye).

A trend of decreasing in strain and increase in crystallite size with substrate temperature was observed. The decrease in strain may indicate the formation of higher quality films at higher substrate temperatures [40]. This could be that at higher temperatures, residual stress of the films relaxes and thus strain is reduced. As with grain size, the increase in substrate temperature increases the mobility of adatoms that also results in the increase of the

crystallite size and crystallinity of the films [41]. This observation is consistent with the increase in grain size observed by SEM. Photoluminescence (PL) studies were carried out for some SnS films to reveal further information on the optical quality of the films and their potential in carrier generation for devices. Figure 6 shows the PL emission spectra of the SnS films with photon excitation at 532 nm.

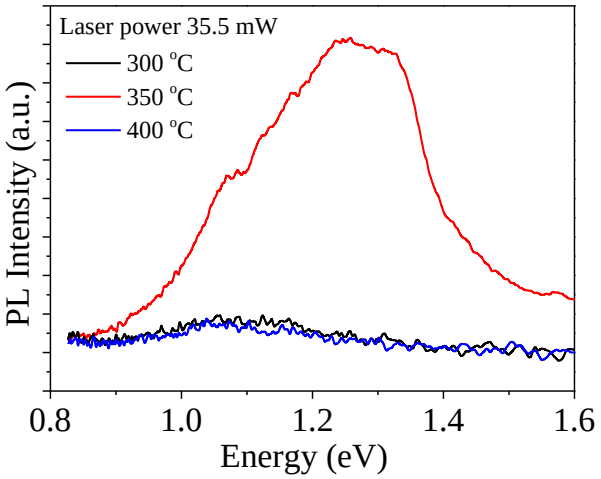

Figure 6: PL spectra of as-deposited SnS films recorded at 6K

SnS film grown at 350 °C has a broad emission peak centred on 1.23 - 1.33 eV, whereas films grown at 300 °C and 400 °C showed no emission peaks. This broad peak has been attributed to emissions from vacancies or defects that are intrinsic to the growth processes of the films [42, 43]. This demonstrates that controlling the film composition and crystal structure to some extend is critical to produce a film that will luminesce, a requisite for any implementation in solar devices.

4. Conclusion

SnS thin films were grown by thermal evaporation onto SLG substrates at varying substrate temperatures. The morphological properties were mildly independent of the growth temperature with a marginal increase in grain size observed. On the other hand, composition, structural and optical properties were strongly influenced by the temperature. A shift in preferred orientation was observed at 300-350°C were the films became aligned along the (040) direction. The single-phase nature of the deposited films was confirmed by both XRD and Raman spectroscopy. A reduction in energy bandgap was observed with increasing substrate temperature and this is strongly related to the loss of Sn in the films. Moreover, it is found that photoluminescence can only be generated for films grown at 350°C which are

stoichiometric and of energy bandgap of 1.37 eV. This study demonstrates that controlling the stoichiometry of the film is key to fabricate future solar devices and future work should focus on improving grain growth in all three directions.

5. Acknowledgements

The authors are grateful to UK-India Education and Research Initiative (UKIERI) for financial support under grants IND/CONT/E/13-14/657 and DST/INT/UK/P-77/2014.

6. References

[1] Sinsersuksakul P, Heo J, Noh W, Hock A S and Gordon R G 2011 Atomic Layer Deposition of Tin Monosulfide Thin Films, *Advanced Energy Materials.* (DOI: 10.1002/aenm.201100330). 1 1116-1125.

[2] Sun L, Haight R, Sinsermsuksakul P, Kim S B, Park H H and Gordon R G 2013 Band alignment of SnS/Zn(O,S) heterojunction in SnS thin film solar cells, *Applied Physics Letters*. 103 181904.

[3] Scragg J J, Dale P J, Peter L M, Zoppi G and Forbes I 2008 New routes to sustainable photovoltaics: evaluation of Cu_2ZnSnS_4 as an alternative absorber material, *Physica Status Solidi (b)* 245 (9) 1772-1778.

[4] Loferski J J 1956 Theroetical considerations governing the choice of the optimum semiconductor for photovoltaic solar energy conversion, *Journal of Applied Physics.* 27 777-784.

[5] Yu L and Zunger A 2012 Identification of potential photovoltaic absorbers based on first-principles of spectroscopic screening of materials, *Physical Review Letters*. 108 068701

[6] Sinsermsuksakul P, Sun L, Lee S W, Park H H, Kim S B, Yang C and Gordon R G 2014 Overcoming Efficiency Limitations of SnS-Based Solar Cells, *Advanced Energy Materials.* 4 1400496.

[7] Sajeesh T H, Jinesh K B, Rao M, Kartha C S and Vijayakumar K P 2012 Defect levels in SnS thin films prepared using chemical spray pyrolysis, *Physica Status Solidi A* 209 7 1274-1278 (DOI 10.1002/pssa.201127442).

[8] Reddy N K, Reddy K T R 2005 SnS films for photovoltaic applications: Physical investigations on sprayed Sn_xS_y films, *Physica B.* 368 25-31.

[9] Sugiyama M, Shimizu T, Kawade D, Ramya K and Reddy K T R 2014 Experimental determination of vacuum-level band alignments of SnS-based solar cells by photoelectron yield spectroscopy, *Journal of Applied Physics*. 115 083508.

[10] Reddy V R M, Gedi S, Pejjai B, Reddy K T R, Zoppi G and Park C 2016 Influence of different substrate on the properties of sulfurized SnS films, *Science of Advanced Materials*. 8 247-251 (doi: 10.1166/sam.2016.2638).

[11] Reddy K T R, Reddy N K and Miles R W 2006 Photovoltaic properties of SnS based solar cells, *Solar Energy Materials and Solar Cells.* 90 3041-3046

[12] Salah H B, Bouzouita H and Rezig B 2005 Preparation and characterisation of tin sulphide thin films by a spray pyrolysis technique, *Thin Solid Films.* 480-481 439-442.

[13] Gunasekaran M and Ichimura M 2007 Photovoltaic cells based on pulsed electrochemically deposited SnS and photochemically deposited CdS and $Cd_{1-x}Zn_xS$, *Solar Energy Materials and Solar Cells*. 91 774-778.

[14] Cheng L L, Liu M H, Wang M X, Wang S C, Wang G D, Zhou Q Y and Chen Z Q 2012 Preparation of SnS films using solid sources deposited by the PECVD method with controllable film characters, *Journal of Alloys and Compounds*. 545 122-129.

[15] Devika M, Reddy N K, Ramesh K, Ganesan R, Gunasekhar K R, Gopal E S R and Reddy K T R 2007 Thickness effect on the physical properties of evaporated SnS films, *Journal of the electrochemical society*. 154 67-73.

[16] Devika M, Reddy K T R, Reddy N K, Ramesh K, Ganesan R, Gopal E S R and Gunasekhar K R 2006 Microstructure dependent physical properties of evaporated tin sulphide films, *Journal of Applied Physics*. 100 023518.

[17] Steinmann V *et al* 2014 3.88% Efficient Tin Sulfide Solar Cells using Congruent Thermal Evaporation, *Advanced Materials.* 26 7488-7492.

[18] Nwofe P A, Reddy K T R, Tan J K, Forbes I and Miles R W 2013 On the Structural and Optical Properties of SnS Films Grown by Thermal Evaporation Method, *Journal of Physics: Conference Series* 417 012039.

[19] Bashkirov S A, Gremenok V F, Ivanov V A, Lazenka V V and Bente K 2012 Tin sulphide thin films and Mo/$_{p}$-SnS/$_{n}$-CdS/ZnO heterojunctions for photovoltaic applications, *Thin Solid Films.* 520 5807-5810.

[20] Park H H *et al* 2014 Co-optimization of SnS absorber and Zn(O,S) buffer materials for improved solar cells, *Progress in Photovoltaic: Research and Applications* ©John Wiley & Sons, Ltd.

[21] Green M A, Hishikawa Y, Dunlop E D, Levi D H, Hohl-Ebinger J and Ho-Baillie A W Y 2018 Solar cell efficiency table (version 51), *Progress in Photovoltaics: Research and Applications*. 26 3-12 (DOI: 10.1002/pip.2978).

[22] Lundberg O, Bodegard M, Malmstrom J and Stolt L 2003 Influence of the Cu(In,Ga)Se_2 Thickness and Ga Grading on Solar Cell Performance, *Progress in Photovoltaics: Research and Applications.* 11 77-88 (DOI: 10.1002/pip.462).

[23] Ramanathan K, Noufi R, To B, Young D L, Bhattacharya R, Contreras M A, Dhere R G and Teeter G 2006 Processing and Properties of Sub-Micron CIGS Solar Cells, *In conference record of the 4th World Conference on Photovoltaic Energy Conversion* 1 380-383.

[24] Han A, Zhang Y, Song W, Li B, Liu W and Sun Y 2012 Structure, morphology and properties of thinned Cu(In, Ga)Se_2 films and solar cells *Semiconductor Science and Technology* 27 035022.

[25] Mathews N R, Garcia C C and Torres I Z 2013 Effect of annealing on structural, optical and electrical properties of pulse electrodeposited tin sulphide films, *Materials Science in semiconductor Processing.* 16 29-37.

[26] Lide D R 2005 ed, CRC Handbook of Chemistry and Physics internet version, *CRC Press Boca Raton, FL*. 6-71.

[27] Martin S, Zoppi G, Aninat R, Forbes I and Guillen C 2013 Study of the Al-grading effect in the crystallization of chalcopyrite Cuin$_{1-x}$Al$_x$Se$_2$ thin films, *Materials Chemistry and Physics.* 140 236-242.

[28] Ogah O E, Zoppi G, Forbes I, and Miles R W 2009 Thin films of tin sulphide for use in thin film solar cell devices, *Thin solid films.* 517 2485-2488.

[29] Guneri E, Gode F, Ulutas C, Kirmizigul F, Altindemir G and Gumus C 2010 Properties of P-type SnS thin films prepared by chemical bath deposition, *Chalcogenide Letters.* 7 685-694.

[30] Yue G H, Peng D L, Yan P X, Wang L S, Wang W and Luo X H 2009 Structure and optical properties of SnS thin film prepared by pulse electrodeposition, *Journal of alloys and compounds.* 468 254-257.

[31] Hassanien A S and Akl A A 2015 Influence of composition on optical and dispersion parameters of thermally evaporated non-crystalline $Cd_{50}S_{50-x}Se_x$ thin films, *Journal of Alloys and Compounds.* 648 280-290.
[32] Ihor S, Mladen K and Mykhailo K 2014 Urbach rule in solid state Physics, *International journal of optics and applications*. 4 76-83.
[33] Kawano Y, Chantana J and Minemoto T 2015 Impact of growth temperature on the properties of SnS film prepared by thermal evaporation and its photovoltaic performance, *Current Applied Physics.* 15 897-901.
[34] Reddy K T R, Nwofe P A and Miles R W 2013 Determination of the minority carrier diffusion length of SnS using electro-optical measurement, *In: Electronic materials letters.* 9 336-366.
[35] Raadik T, Grossberg M, Raudoja J, Traksmaa R, Krustok J, 2013 Temperature dependent photo reflectance of SnS crystals, *Journal of Physics and Chemistry of solids*. 74 1683-1685.
[36] Ballipinar F and Rastogi AC 2017 Tin sulfide (SnS) semiconductor photo-absorber thin film for solar cells by vapour phase sulfurization of Sn metallic layers using organic sulfur source, *Journal of Alloys and Compounds.* 728 179-188.
[37] Mare S D, Menossi D, Salavei A, Artegiani E, Piccinelli F, Kumar A, Mariotto G and Romeo A 2017 SnS thin film solar cells: perspectives and limitations, *Coatings*. 7 34.
[38] Zoppi G, Durose K, Irvine S J C and Barrioz V 2006 Grain and crystal texture properties of absorber layers in MOCVD-grown CdTe/CdS solar cells, *Semiconductor science and technology*. 21 763-770.
[39] Monte V D, Purushotham Y and Dole B N 2012 Williams-Hall analysis in estimation of lattice strain in nanometer-sized ZnO particles, *Journal of Theoretical and Applied Physics.* 6 6.
[40] Lalitha S, Sathyamoorthy R, Senthilarasu S, Subbarayan A and Natarajan K 2004 Characterisation of CdTe thin film dependence of structural and optical properties on temperature and thickness, *Solar energy materials and solar cells*. 82 187-199.
[41] Sathyamoorthy R, Narayandass S K and Mangalaraj D 2003 Effect of substrate temperature on the structure and optical properties of CdTe thin film, *Solar energy materials and solar cells.* 76 339-346.
[42] Ghosh B, Das M, Banerjee P and Das S 2008 Fabrication and optical properties of SnS thin films by SILAR method, *Applied Surface Science.* 254 6436-6440.
[43] Sajeesh T H, Poornima N, Kartha C S and Vijayakumar K P 2010 Unveiling the defect levels in SnS thin films for photovoltaic applications using photoluminescence technique, *Physica Status Solidi A*. 207 1934-1939.

6. Supplementary information

Table S1: Texture coefficient (C_{hkl}) and degree of preferred orientation (σ) across the temperature.

Substrate temp. (^oC)	$C_{(hkl)}$ (110)	(120)	(021)	(101)	(111)	(040)	(141)	(211)	σ
200	1.769	1.234	0.352	1.165	1.863	0	0.357	0.431	0.56
250	1.183	0.691	0.168	1.26	1.932	0	0.436	0.344	0.56
300	1.972	0.957	0.288	0.751	2.341	0	0.319	0.437	0.79
350	0.199	0.222	0.063	0.082	0.619	7.216	0.029	0.05	2.33

400	0.165	0.219	0.095	0.07	0.517	7.432	0.042	0.037	2.41

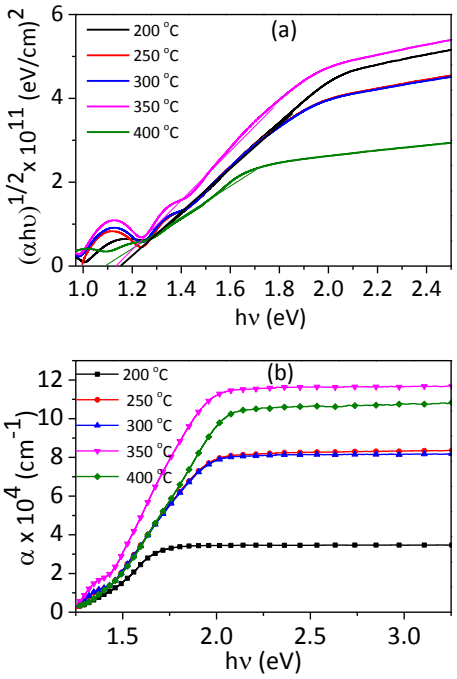

Figure S1: (a) $(\alpha h\nu)^{1/2}$ and (b) absorption coefficient (α) against photon energy.

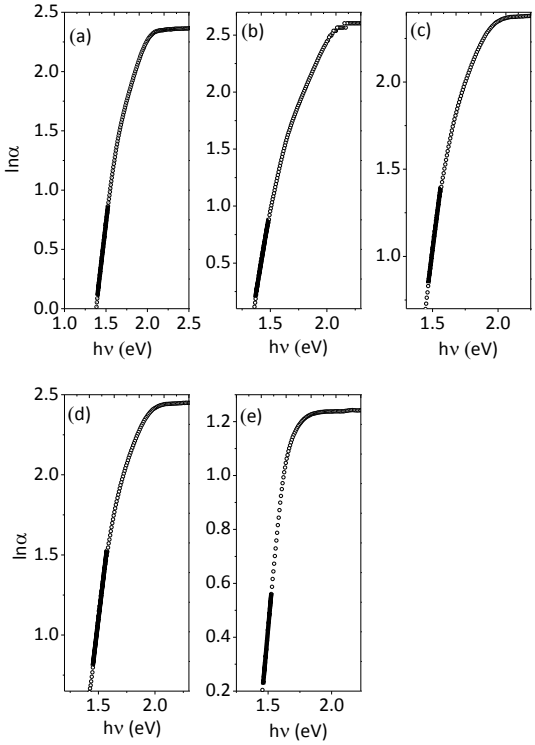

Figure S2: Plot of lnα versus $h\nu$ of the as-deposited SnS thin films at (a) 200 ºC, (b) 250 ºC, (c) 300 ºC, (d) 350 ºC and (e) 400 ºC substrate temperature.